Propagating Alfvén waves in open structures with random structuring

D. J. Pascoe [●],[1]★ I. De Moortel,[1,2] P. Pagano[3,4] and T. A. Howson[1]

[1]*School of Mathematics and Statistics, University of St Andrews, St Andrews, Fife KY16 9SS, UK*
[2]*Rosseland Centre for Solar Physics, University of Oslo, PO Box 1029 Blindern, NO-0315 Oslo, Norway*
[3]*Dipartimento di Fisica & Chimica, Università di Palermo, Piazza del Parlamento 1, I-90134 Palermo, Italy*
[4]*INAF-Osservatorio Astronomico di Palermo, Piazza del Parlamento 1, I-90134 Palermo, Italy*

ABSTRACT

We consider the behaviour of Alfvén waves propagating in a medium with random density perturbations. The imposed density perturbations have a broad-band spectrum and their characteristic spatial scale may be defined according to the peak in the spectrum. The interaction of the boundary driven Alfvén waves with the medium generates reflections most efficiently when their wavelength is comparable to the spatial scale of the density perturbations. For our monotonic driver, this leads to the generation of quasi-periodic oscillations. The periods of oscillation of the propagating Alfvén waves is no longer only associated with the driver. Additional periodicities may be associated with one or more characteristic spatial scales in the density profile, or with beating between other spectral components. Multiple wave reflections cause oscillatory power to be retained at low altitudes, increasing opportunities to contribute to heating at those locations.

Key words: MHD – Sun: atmosphere – Sun: corona – Sun: oscillations.

1 INTRODUCTION

Observations have revealed that magnetohydrodynamic (MHD) waves are ubiquitous in the solar atmosphere. Propagating transverse waves have been detected in the chromosphere using Hinode (De Pontieu et al. 2007; Okamoto et al. 2007), and in the corona using the Coronal Multi-channel Polarimeter (CoMP; Tomczyk et al. 2007). Such waves attract attention both as a diagnostic technique (e.g. Nakariakov et al. 2021; Anfinogentov et al. 2022) and as a potential source of coronal heating (e.g. Van Doorsselaere et al. 2020) and solar wind acceleration (e.g. van Ballegooijen & Asgari-Targhi 2016).

In closed structures such as coronal loops, waves are efficiently trapped and periodic transverse displacements have been interpreted as kink oscillations (e.g. Nakariakov et al. 2021). Their damping and dissipation through processes of resonant absorption (e.g. Ionson 1978), phase mixing (Heyvaerts & Priest 1983), and the Kelvin–Helmholtz instability (KHI; e.g. Terradas et al. 2008b) have been studied in detail. The damping rate of large amplitude kink oscillations, impulsively excited by flares or CMEs, is frequently used for coronal seismology as a diagnostic for the properties of the particular plasma structure. Decayless oscillations are also observed to be ubiquitous in coronal loops (Anfinogentov, Nakariakov & Nisticò 2015), suggesting a continuous source of wave energy, such as photospheric motions. The ubiquitous propagating waves observed in the corona (e.g. Tomczyk et al. 2007) may also be associated with the same energy source as ubiquitous decayless oscillations, such as random footpoint motions (Afanasyev, Van Doorsselaere & Nakariakov 2020).

Fast and Alfvén waves driven by azimuthal footpoint motions have been investigated for periodic (De Groof, Paes & Goossens 2002) and random (De Groof & Goossens 2002) drivers. Wave heating of coronal loops due to azimuthally polarized footpoint motions has been studied by Berghmans & Tirry (1997) for dissipative MHD and by Tirry & Berghmans (1997) for ideal MHD. Radially polarized footpoint motions were considered for an ideal slab model by Tirry, Berghmans & Goossens (1997) and De Groof & Goossens (2000).

Waves are also frequently observed in open coronal structures (e.g. review by Banerjee et al. 2021). Furthermore, coronal heating is not confined to closed structures. The potential for propagating waves to account for, or contribute to, heating in open structures is based on the wave energy present in such waves, and the opportunity for that energy to be dissipated at the appropriate locations. For Alfvén waves in open structures, turbulence is often invoked to provide efficient dissipation of the wave energy (e.g. Cranmer & van Ballegooijen 2005; van Ballegooijen et al. 2011; Asgari-Targhi et al. 2021).

Murawski, Nakariakov & Pelinovsky (2001a) considered the propagation of fast MHD waves in a randomly structured medium in the context of global EIT waves. This scenario was also considered by Yuan et al. (2015), who studied the case of short (Gaussian) fast MHD pulses propagating in a random medium. The interaction of the wave with the medium causes the generation of quasi-periodic waves (e.g. Nakariakov, Pascoe & Arber 2005) and the attenuation of the initial pulse. The effect of random structuring has also been considered for acoustic waves, where space-dependent random profiles again cause attenuation (Medrek et al. 2002), though time-dependent random fields can cause wave amplification for structuring is in density (Murawski, Nocera & Mědrek 2001b; Nocera, Medrek & Murawski 2001) or velocity profiles (Murawski & Medrek 2003a; Murawski 2004).

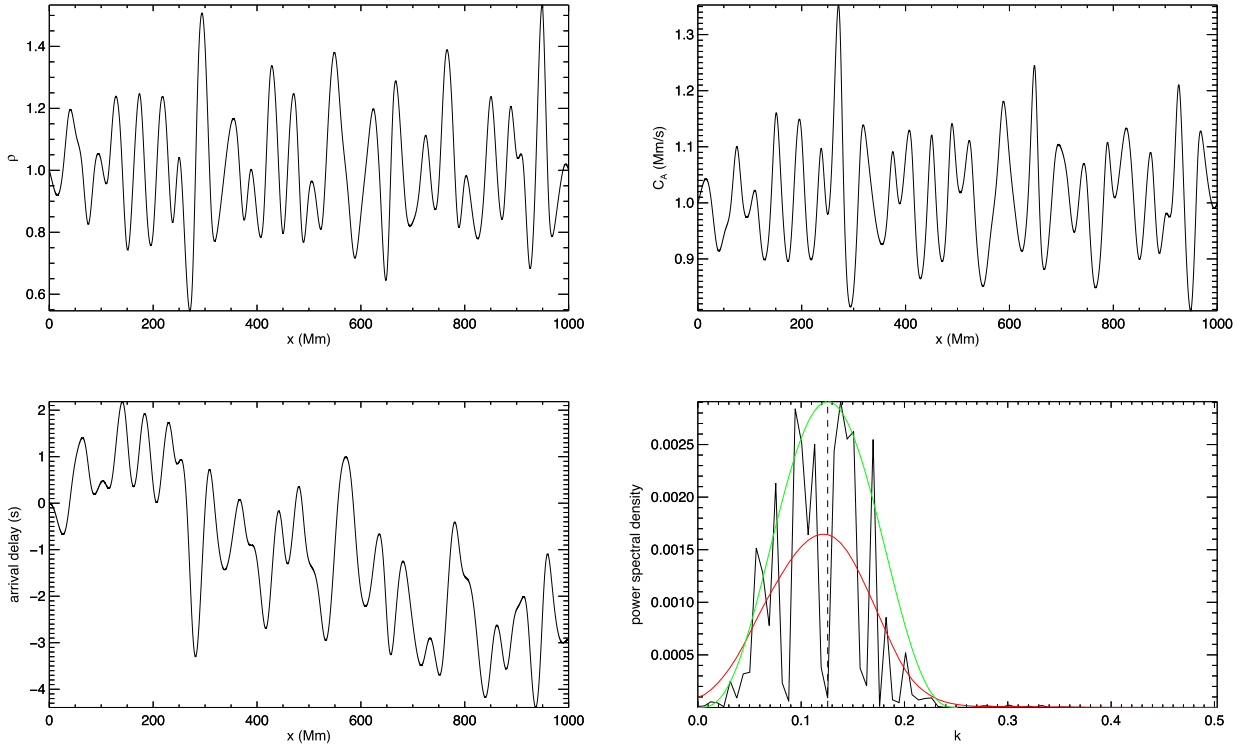★ E-mail: david.pascoe@st-andrews.ac.uk

Figure 1. Example of random density profile with $\lambda_s = 50$ Mm. The top panels show the profiles of the plasma density and Alfvén speed. The bottom left panel shows the arrival delay for a propagating wave in comparison to a uniform medium, given by equation (1). The bottom right panel shows the Fourier power spectrum of the structured medium (red line is the same spectrum with Tukey smoothing). The vertical dashed line corresponds to $k_s = 2\pi/\lambda_s$ and the green line represents the source power spectrum.

In this paper, we consider the propagation of transverse MHD waves through a plasma with random density perturbations which have a characteristic spatial scale that can be varied. We consider propagation in open coronal structures for which the direction of wave propagation is aligned with the magnetic field, rather than perpendicular as in Murawski et al. (2001a) and Yuan et al. (2015), although we can expect similar results for low amplitude waves that are described by the same linear wave equation. We examine the presence of longitudinal structuring of the plasma density, i.e. the variation of the Alfvén speed in the direction of wave propagation. To isolate the effect of longitudinal structuring we do not consider the presence of transverse structuring, which can have a significant effect on the dissipation of wave energy and for which the characteristic spatial scale may be determined independently of longitudinal structuring, and so we exclude dissipative effects generally. This paper is organized as follows. We describe our model in Section 2 and present the results of our parametric study in Section 3. Our focus is on the trapping of wave energy and the generation of additional periodicities due to the presence of the random perturbations. Further discussion is presented in Section 4, with conclusions in Section 5.

2 MODEL

We perform a parametric study to investigate the behaviour of Alfvén waves propagating in a medium with random density perturbations. The period of our monotonic boundary driver is $P_d = 60$ s and so for an average Alfvén speed of 1 Mm s^{-1}, the wavelength of the driven Alfvén wave is $\lambda_d = 60$ Mm. A key parameter of our model is the characteristic spatial scale of the density perturbations λ_s.

In Yuan et al. (2015), the randomly structured medium is generated by a method based on summing sinusoidal perturbations. The sinusoidal perturbations correspond to the spatial harmonics of the numerical domain and increasing the number of harmonics leads to shorter spatial scales being introduced. The correlation length that characterizes the random medium is then defined as the full width at half-maximum of the autocorrelation coefficient of the density profile. In this paper, we generate our random density profiles by using the desired power spectrum to define the weighting of random Fourier components. The profile of the random perturbations is then obtained as the inverse Fourier transform. This method is described in Timmer & Koenig (1995) for the case of a time-series with a power-law spectrum. In our case, the proposed power spectrum is based on a beta distribution and is qualitatively similar to a Gaussian distribution but defined on a finite interval. This method allows us to define the desired characteristic scale of the density perturbations directly, rather than constructing a random profile and calculating the corresponding scale afterwards.

Fig. 1 shows an example of a random density profile used in our simulations with $\lambda_s = 50$ Mm. The top left panel shows the density (in normalized units) with the corresponding Alfvén speed in the top right panel. For all simulations, the standard deviation of the amplitude of the random perturbations is 20 per cent of the background value. For convenience, we also impose that the perturbations tend to zero at the boundary of the region of interest (i.e. $\rho = 1$ at $x = 0$ and $x = 1000$ Mm). The bottom left panel shows the delay to a wave that propagates at the local Alfvén speed. The delay is calculated as the arrival time in the structured medium in comparison to a uniform medium with $C_A = 1$ Mm s^{-1}. For propagation at the
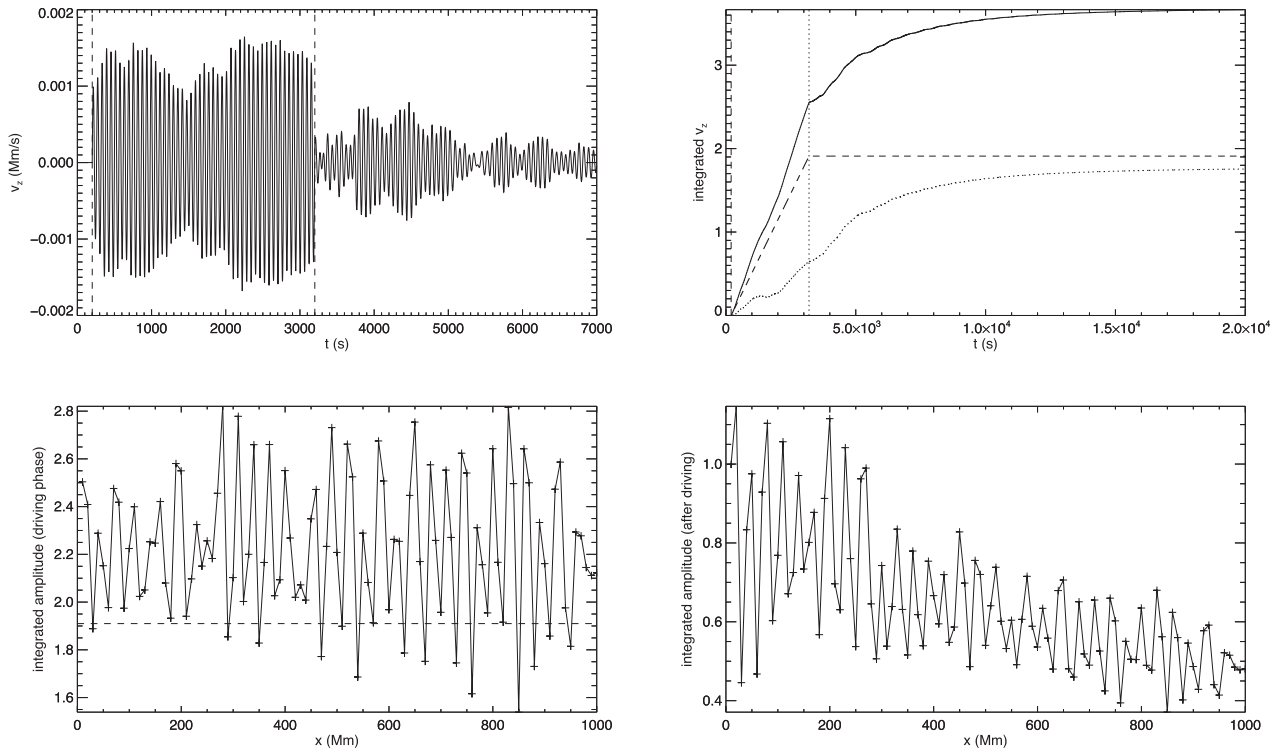
Figure 2. Example of Alfvén wave velocity time-series (top left). The top right panel shows the Alfvén wave amplitude integrated in time. The dashed line is the theoretical value for a uniform medium that increases until the end of the driving phase (vertical dotted line). The dotted curve is the difference between the actual integrated amplitude and that for the uniform medium. The bottom panels show the spatial variation of the wave amplitude, calculated by integrating its absolute value for times during (left) and after (right) the driving phase. The horizontal dashed line corresponds to the value in a uniform medium.

local Alfvén speed $C_A(x)$ the arrival time at a distance d is

$$t(d) = \int_0^d \frac{1}{C_A(x)}\, dx. \qquad (1)$$

The delay for a particular position is determined by the preceding random structures but is always negative, implying wave acceleration compared with a uniform medium, by the end of the profile where the density perturbations average to zero but there is a net increase in the average wave speed (e.g. Murawski & Medrek 2003b). The bottom right panel shows the Fourier power spectrum of the structured medium (red line is the same spectrum with Tukey smoothing). The vertical dashed line corresponds to $k_s = 2\pi/\lambda_s$. It is evident from the spectrum that the peak corresponds to the proposed characteristic spatial scale but is also sufficiently broad that the density profile does not simply appear as a sinusoidal oscillation.

We perform simulations using LARE2D (Arber et al. 2001) that solves the 2.5D non-linear visco-resistive MHD equations. In this study, our choice of equilibrium and driver corresponds to a 1D problem of propagating Alfvén waves. The magnetic field is constant and in the x-direction. The particular density profile is set to be in equilibrium by varying the temperature to satisfy the condition of total pressure balance (with a plasma $\beta = 0.1$). We drive transverse waves at the lower boundary ($x = 0$) with the z component of the velocity, using

$$v_z = A_0 \sin(\omega t), \qquad (2)$$

where A_0 is the wave amplitude, and $\omega = 2\pi/P_d$ is the frequency. This injects Alfvén waves into the domain. The y and z directions are both invariant throughout the simulations ($\partial/\partial z \equiv 0$ in LARE2D,

and our model further imposes $\partial/\partial y \equiv 0$). The amplitude of the driver $A_0 = 0.001$ Mm s^{-1} is chosen to be sufficiently small to approximate the linear regime and avoid the non-linear generation of density perturbations. The driver is applied for 3000 s which corresponds to 50 cycles. Our use of this extended driving time means we have a well-defined period associated with the driven Alfvén wave. In comparison, a short pulse such as that used in Yuan et al. (2015) corresponds to a broad-band spectrum. This well defined and constant period assists our analysis of additional periodicities generated by the random structuring (see Section 3.2).

An open upper boundary is simulated using an extended damping layer. The region of interest that contains random density perturbations is $x = [0, 1000]$ Mm, while the full numerical domain extends to 3000 Mm. Outside the region of interest, velocity perturbations are artificially damped to ensure there are no reflections from the upper boundary. The domain is simulated using 30 000 grid points and an end time of 20 000 s. We note that our choice of normalization is arbitrary and corresponds to typical spatial and temporal scales for MHD waves in the solar corona.

3 RESULTS

Our study is comprised of numerous numerical simulations with different values of structuring wavelength λ_s and different values of the seed used in the pseudo-random number generator for the density profile perturbations. We focus on analysing two effects in this section; the retention of wave energy by the random structuring, and the period(s) of oscillation of the Alfvén waves.
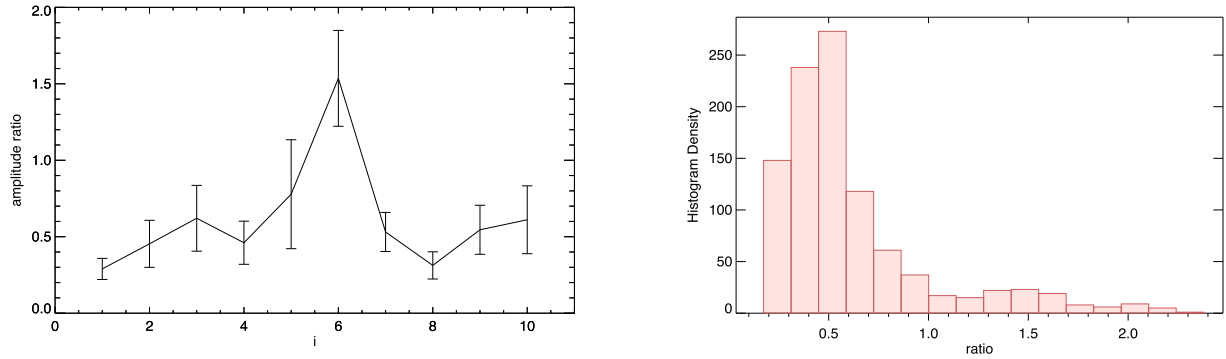
Figure 3. Collation of results for simulations with different random seeds. The simulations are summarized by the integrated wave amplitude after the driving phase compared to the initial input by the driver.

3.1 Trapping of wave energy

For each of our numerical simulations, we use 100 spatial probes uniformly distributed throughout the region of interest to examine the wave behaviour. The probes feature of LARE2D allows efficient output of plasma parameters with maximal temporal resolution i.e. we only output at 100 locations in the *x*-direction rather than the full numerical resolution of 30 000 grid points. The plasma parameters at the probe locations are output at every internal time-step (as determined in accordance with the CFL condition) that is typically far higher than we require in this study and so the data are resampled by interpolating to a fixed interval of 1 s before further analysis.

To examine the behaviour of Alfvén waves, we focus on the time-series for the transverse plasma velocity v_z. An example of the output from an individual probe, located 200 Mm from the driven boundary, is shown in the top left panel of Fig. 2. The full time-series has a duration of 20 000 s but is truncated here for clarity. The two vertical dashed lines correspond to the arrival times of the start and end of the driven oscillation (at this height), given by equation (1). For this particular simulation, weak reflections are generated by the random density structuring and so the driven oscillation is readily distinguished from the later oscillations generated by reflections by the significant decrease in amplitude. This particular probe is located near a local minimum in the density profile and so during the driven phase the amplitude is typically higher than the driver amplitude ($A_0 = 0.001$ Mm s^{-1}).

The top right panel of Fig. 2 shows the absolute value of the Alfvén wave amplitude integrated in time,

$$A(t) = \int_0^t |v_z| \mathrm{d}t, \tag{3}$$

with the difference that arises due to the effect of reflections denoted by the dotted line. For this particular case, the difference is always positive. However, for scenarios in which there is destructive interference between the driven and reflected waves the difference may be negative for early times.

We can estimate the typical amplitude during the driven phase by integrating the absolute value of v_z in time for each spatial probe, as shown in the bottom left panel of Fig. 2. The horizontal dashed line corresponds to the expected value for a uniform medium based on the driver amplitude and frequency. The bottom right panel of Fig. 2 shows the same estimated amplitude after the driven phase (for which the expected value for a uniform medium would be zero). Unlike the previous panel, the reflected amplitude is typically larger for probes located closer to the driven boundary due to the greater opportunities for reflected waves to contribute to the time-series there. The value

for consecutive probes can vary according to the particular details of wave interference.

To capture the behaviour of an individual simulation we consider the mean value of this integrated wave amplitude remaining after the driving phase. The result is presented as a ratio where the integrated wave amplitude is normalized by the value corresponding to the driver. Hence, a ratio of 1 implies the reflections have effectively doubled the lifetime of the wave within the region of interest.

Fig. 3 shows the results collated for 10 numerical simulations, each with the same nominal value of $\lambda_s = 50$ Mm but with a different seed for the pseudo-random number generator. Owing to the details of the particular random sequence, the actual peak(s) in the generated density profile spectrum may differ slightly from the nominal value requested by the user. We find that the details of the random structuring can have a significant effect on the efficiency of the reflections. The left-hand panel of Fig. 3 shows the results grouped by simulation; for each of the 10 different random seeds the plotted amplitude ratio represents the mean value calculated over all 100 probes, and the error bars correspond to the first and third quartiles. We note that the labelling of the 10 simulations $i = [1, 10]$ is arbitrary. The right-hand panel is a histogram of the same data representing the mean value for each of the 1000 probes (10 simulations each with 100 probes). The histogram exhibits a peak value ≈0.5 with a long tail, most of which can be attributed to one particular simulation ($i = 6$ in Fig. 3) in this case. Whether the peak value or the tail is most important or representative for scenarios relevant to coronal heating remains an open question, though we note that such extreme cases of wave trapping may arise due to our use of a monochromatic driver whereas a more realistic driver is unlikely to be so stable (see further discussion in Section 4).

Fig. 4 shows the summary of results for different values of the nominal structuring scale λ_s. The solid line represents the mean value of the amplitude ratio, while the lower and upper dashed lines represent the first and third quartiles, respectively. The peak in each curve occurs at $\lambda_s = 30$ Mm which is related to our choice of driving period $P_d = 60$ s. For this driving period, this represents the spatial scale most likely to generate efficient reflections, although as previously noted this is the nominal spatial scale requested by the user (i.e. not accounting for random variations). This result is consistent with that found for a short pulse by Yuan et al. (2015) for which reflection was found to be most efficient when the correlation length was half of the initial pulse width. For small values of λ_s (compared to the wavelength of the driven wave), the random structuring appears as fine structuring that MHD waves are typically insensitive to (e.g. Pascoe, Nakariakov & Arber 2007; Terradas et al. 2008a). At the
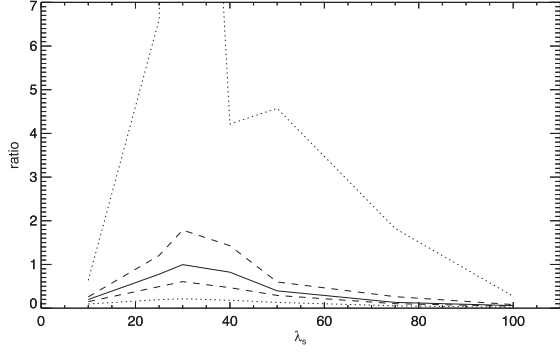
Figure 4. Dependence of the wave amplitude ratio on the nominal structuring spatial scale λ_s. The solid line represents the mean value of the amplitude ratio, while the lower and upper dashed lines represent the first and third quartiles. The lower and upper dotted lines represent the minimal and maximal values.

other extreme of very large λ_s, the structuring corresponds to a slowly varying medium, lacking strong gradients in the Alfvén speed that promote reflections.

3.2 Generation of periodicities

As described in Section 2, we generate our random structure based on a proposed spatial scale λ_s, with a corresponding wavenumber $k_s = 2\pi/\lambda_s$. We can consider a periodicity associated with this spatial scale of $P_s = 2\lambda_s/C_A$. As shown in the example in Fig. 1, the density profile spectrum is typically broad (to avoid having a monochromatic spectrum corresponding to sinusoidal perturbations). In other cases, depending on the particular details of the random density perturbations, the spectrum may feature multiple strong peaks distributed

around the nominal wavenumber k_s. More generally, we can consider a range of periodicities associated with the spectrum of the random structuring.

In this section, we present several different cases of additional periodicities generated by the interaction of the Alfvén waves with the random density structuring.

At times during the driving phase of the simulation, the oscillations detected at each probe location are dominated by the period of the driver. An example of a time-series (top-left panel) and corresponding power spectrum (bottom-left panel) is shown in Fig. 5 for a probe at $x = 200$ Mm in a simulation with $\lambda_s = 100$ Mm. For this large structuring scale, the period associated with the random structuring (red curve) is distinct from that of the driver (vertical dashed line), although the interaction is weak and so the wave amplitudes are small (see also Fig. 4). The blue vertical dot–dashed line corresponds to the beating frequency i.e. the average of the frequencies of the driver and that associated with the structure. The top right panel of Fig. 5 shows the signal at the same probe, starting after the driven waves and their immediate reflections have passed (taken to be twice the time for the directly driven waves to have passed). Fig. 6 shows this later velocity power spectrum calculated for each of the 100 simulation probe locations. Each spectrum is normalized to its own maximum to remove the variation in amplitude between probes (see e.g. the variation in the bottom right panel of Fig. 2). The spectra demonstrate that the period of oscillation which is associated with the random perturbations is consistent for different locations.

In the example above, the spectrum of the density profile perturbations was well approximated as a single, broad peak. The example in Fig. 7 shows a scenario for which the spectrum associated with the random density perturbations has two peaks (corresponding to spatial scales either side of the nominal value $\lambda_s = 50$ Mm). In this
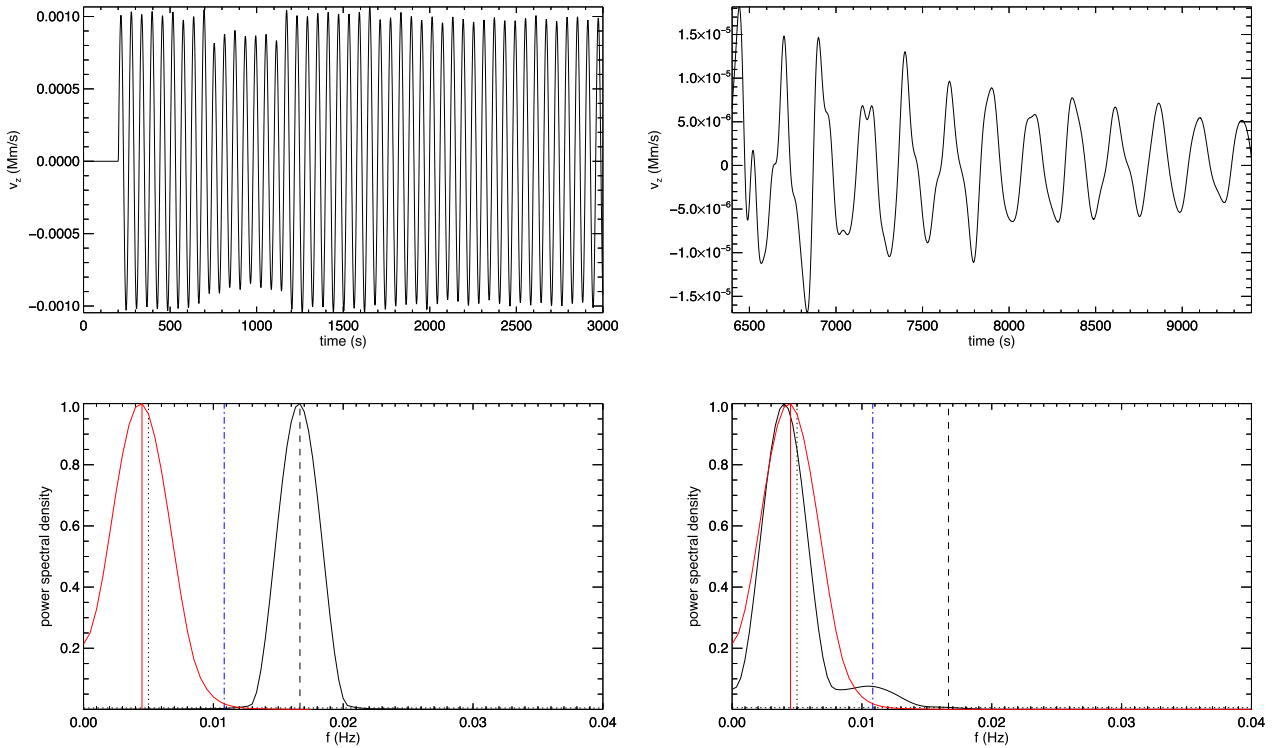
Figure 5. Examples of velocity profiles (top) taken during the driving phase of the simulation (left) and at a later time (right). The corresponding power spectra (bottom) are shown by the black curves. The red curves represent the periodicity associated, with the random structure with the dotted line corresponding to the nominal structuring spatial scale λ_s. The dashed and dot–dashed lines correspond to the driver and beating frequencies, respectively.
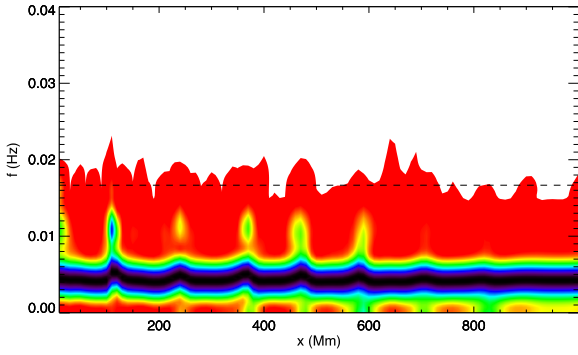
Figure 6. Velocity power spectra calculated for each probe location. The horizontal dashed line corresponds to the period of the driver. The spectrum for each probe is normalized to its maximum to remove the variation in amplitude between probes.
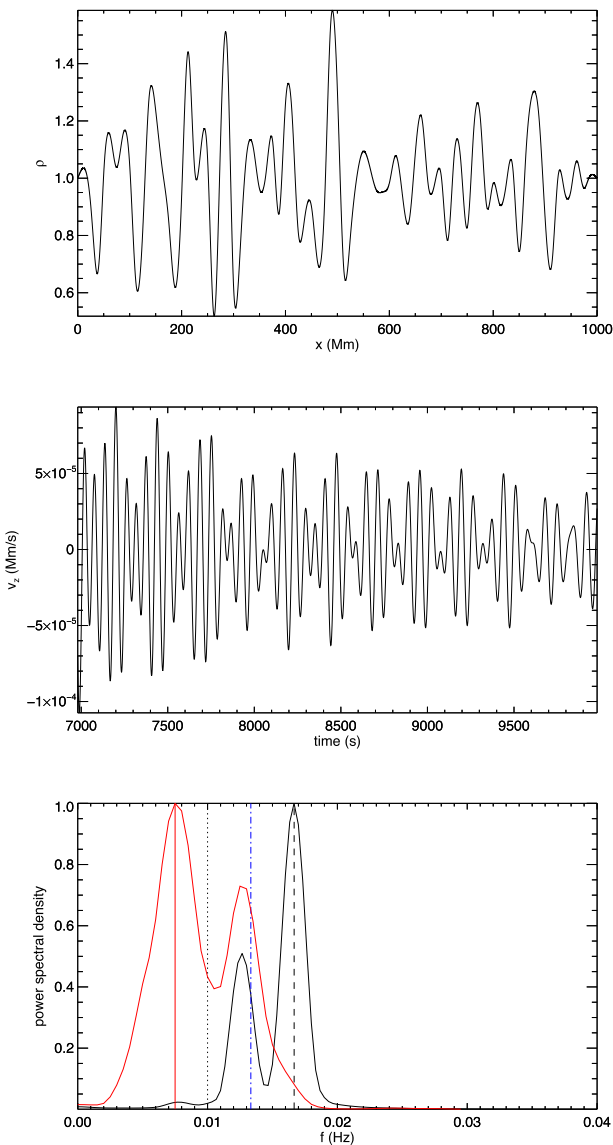

Figure 7. Example of a density profile that features two dominant spectral components (top panel). The middle panel shows an example velocity profile, with the corresponding spectrum shown by the black curve in the bottom panel. The red curve shows the spectral profile associated with the density perturbations.

case, the lower λ_s (in comparison to the previous example of $\lambda_s = 100$ Mm) is more favourable for interaction with the driven waves, i.e. closer to the peak value of 30 Mm, and so the reflected wave energy is significantly larger. A strong peak in the power spectrum corresponding to the reflected driven waves persists long after the directly driven waves have passed. There is a second strong peak in the velocity power spectrum of $f \approx 0.0125$ Hz which is associated with a particular spatial scale present in the plasma density profile. We note that this is not the dominant spectral component of the density profile, but is instead the one which is most similar to the frequency of the driver. There is also a peak in the velocity power spectrum corresponding to the other density profile periodicity although its amplitude is negligible.

These results suggest possible seismological applications to investigate the plasma properties of open magnetic structures by demonstrating that the periodicities present in the system are determined by the longitudinal structuring in addition to the initial wave source. However, it is evident that caution is required in interpreting the detected periodicities since the previous two examples demonstrate that periodicities may be due to several different factors: they may be associated with the footpoint driver; they may correspond to a characteristic scale present in the medium (though not necessarily the dominant one); or may be an average of two such periodicities generated by beating. We also note that application of our numerical results to observable data would be aided by forward modelling synthetic signals corresponding to the particular data product.

4 DISCUSSION

Here, we consider a particular simulation we noted as having very efficient reflections (top left panel). This is one of our simulations with $\lambda_s = 30$ Mm, where the interaction is typically strongest, but for this specific case the trapping of wave energy is significantly greater than others. The generation of large amplitudes (greater than the amplitude of the driver) is due to constructive interference of the reflected waves. We demonstrate this by repeating the simulation with a numerical domain which is extended by $\lambda_d/4 = 15$ Mm near the lower, driven footpoint. In this additional region, the medium is uniform so its only effect is to introduce a phase shift, compared with the previous simulation, as the driven waves encounter the density perturbations. In this case (top right panel), we obtain velocity perturbations that are significantly lower, both during and after the driving phase.

The scenario with significant constructive interference is therefore a consequence of the particular details of the random medium but also due to the period of our driver being exactly constant (no changes in phase). We can further demonstrate this effect by varying the period of oscillation during the driving phase; the bottom left panel of Fig. 8 shows the case of the period increasing linearly in time from 0.9 $P_d = 54$ s to 1.1 $P_d = 66$ s over the driving time of 3000 s. The bottom right panel shows the case of the period decreasing between the same limits during the driving phase. In both scenarios, the typical amplitude is between the more extreme cases presented in the top panels. We therefore caution against the use of a monochromatic driver in numerical simulations due to the potential for misleading results based on the sensitivity to the details of random structuring.

In the solar atmosphere, the driving due to random footpoint motions is unlikely to have a monochromatic spectrum. The random density perturbations will also vary in time due to non-linear (e.g. ponderomotive motions, KHI) and non-ideal processes (e.g. heating). The range of behaviours present in our various simulations therefore represent different conditions which may be satisfied at different
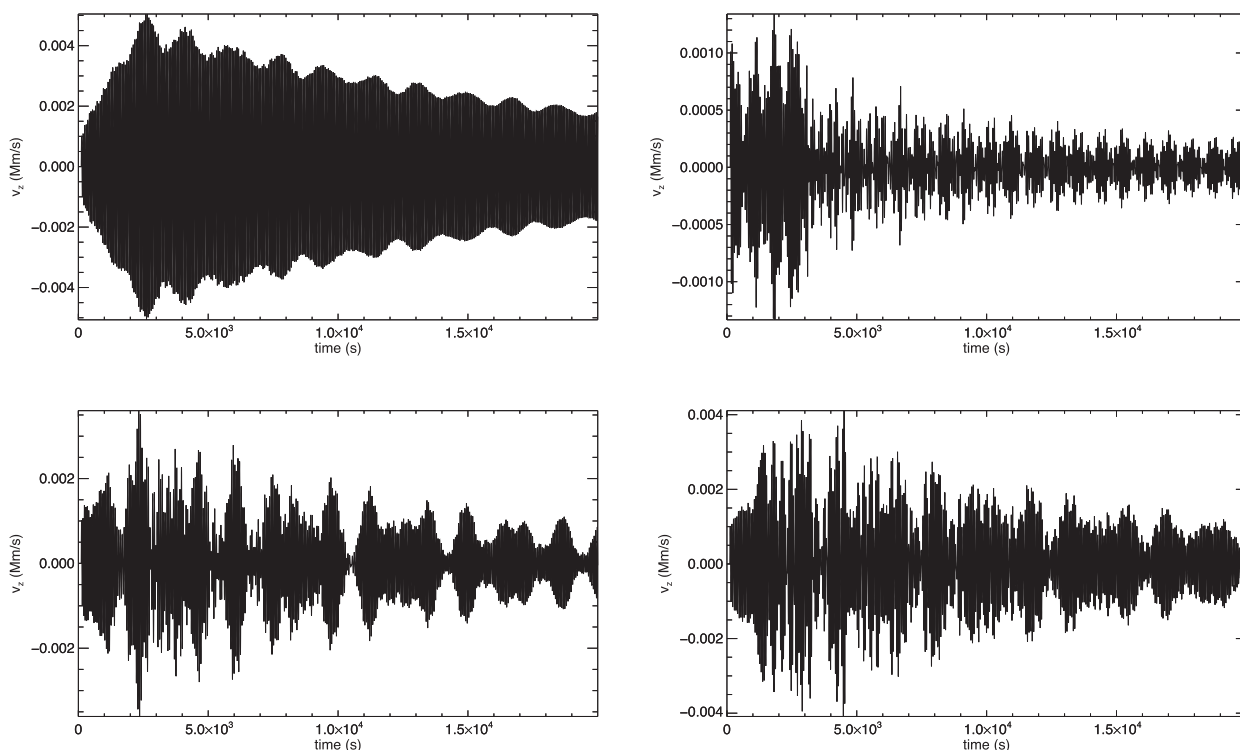
Figure 8. Velocity profile for case of particularly efficient wave trapping (top left). The top right panel shows the equivalent result when the location of the driven boundary is shifted relative to the density perturbations. The bottom panels show the effect of replacing the constant period driver with an increasing (left) or decreasing (right) value.

times. Based on Fig. 4, we can expect that reflections typically increase the lifetime of propagating waves in the region of interest by up to 2–3 times (corresponding to a ratio of 1–1.5), but also occasionally by a significantly greater factor when conditions are favourable.

We may consider the implications of our results for the potential of wave heating by propagating waves in a randomly structured medium. We have demonstrated that modest (20 per cent standard deviation) density perturbations are capable of significantly extending the lifetime of propagating waves within some region of interest. More heating could occur at lower heights than would do so in a comparable uniform medium since additional wave energy that would escape the region of interest without reflections remains available for dissipation, but even so only under certain conditions (see next paragraph about Poynting flux). In the case of weakly non-linear driven waves, the constructive interference by reflections may also enhance non-linear dissipation mechanisms. On the other hand, the reflected waves will modify the Poynting flux injected by the wave driver. Unless the driving happens to be resonant with the returning modes, the mean energy injection rate will decrease (see e.g. Prokopyszyn & Hood 2019; Prokopyszyn, Hood & De Moortel 2019). Consequently, the trapping of energy through wave reflections does not necessarily lead to a similar increase in the heating rate at low altitudes.

In Section 3.2, we demonstrated that additional periodicities associated with the random structuring can be generated, for which some frequency-dependent damping mechanism may be stronger. However, typically only a small fraction of the driven wave energy is contained in these oscillations. The increased exposure of the waves to some damping mechanism at lower heights may therefore be the most significant effect.

5 CONCLUSIONS

The propagation of waves through a medium with random (density) structuring will generally lead to reflections. This has previously been shown to generate quasi-periodic oscillations from an initial pulse. In this paper, we consider the effect in terms of trapping wave energy at lower heights as it provides greater opportunities for heating (although we do not study heating directly in our ideal simulations).

We considered density structures that have a characteristic spatial scale (λ_s) associated with them. Interaction with propagating waves is greatest for wavelengths that are comparable to λ_s. From our parametric study, we demonstrated that the retention of wave energy depends on the wavelength of the driven waves in comparison to the spatial scale λ_s. There can be significant differences between particular instances of the random structuring, but the greatest interactions are typically found with $\lambda_d = 2\lambda_s$. This is consistent with the result found by Yuan et al. (2015) for the case of a fast MHD wave pulse in a randomly structured medium.

We have demonstrated that periodicities can occur in addition to that of the initial driver; the period of the driver, persisting after the driver is turned off due to trapping of waves by reflection; a periodicity associated with the random structuring (most clearly demonstrated when sufficiently far from the driver period although this also corresponds to weaker reflections); and the beating period which is an average of the previous two periods.

DATA AVAILABILITY

The data from the numerical simulations and analysis presented in this paper are available from the corresponding author upon reasonable request.

REFERENCES

Afanasyev A. N., Van Doorsselaere T., Nakariakov V. M., 2020, A&A, 633, L8
Anfinogentov S. A., Nakariakov V. M., Nisticò G., 2015, A&A, 583, A136
Anfinogentov S. A. et al., 2022, Space Sci. Rev., 218, 9
Arber T., Longbottom A., Gerrard C., Milne A., 2001, J. Comput. Phys., 171, 151
Asgari-Targhi M., Asgari-Targhi A., Hahn M., Savin D. W., 2021, ApJ, 911, 63
Banerjee D. et al., 2021, Space Sci. Rev., 217, 76
Berghmans D., Tirry W. J., 1997, A&A, 325, 318
Cranmer S. R., van Ballegooijen A. A., 2005, ApJS, 156, 265
De Groof A., Goossens M., 2000, A&A, 356, 724
De Groof A., Goossens M., 2002, A&A, 386, 691
De Groof A., Paes K., Goossens M., 2002, A&A, 386, 681
De Pontieu B. et al., 2007, Science, 318, 1574
Heyvaerts J., Priest E. R., 1983, A&A, 117, 220
Ionson J. A., 1978, ApJ, 226, 650
Medrek M., Michalczyk J., Murawski K., Nocera L., 2002, Waves Random Media, 12, 211
Murawski K., 2004, Waves Random Media, 14, 467
Murawski K., Medrek M., 2003a, Waves Random Media, 13, 287
Murawski K., Medrek M., 2003b, Waves Random Media, 13, 311
Murawski K., Nakariakov V. M., Pelinovsky E. N., 2001a, A&A, 366, 306
Murawski K., Nocera L., Mědrek M., 2001b, A&A, 376, 708
Nakariakov V. M., Pascoe D. J., Arber T. D., 2005, Space Sci. Rev., 121, 115
Nakariakov V. M. et al., 2021, Space Sci. Rev., 217, 73
Nocera L., Medrek M., Murawski K., 2001, A&A, 373, 301
Okamoto T. J. et al., 2007, Science, 318, 1577
Pascoe D. J., Nakariakov V. M., Arber T. D., 2007, Sol. Phys., 246, 165
Prokopyszyn A. P. K., Hood A. W., 2019, A&A, 632, A93
Prokopyszyn A. P. K., Hood A. W., De Moortel I., 2019, A&A, 624, A90
Terradas J., Arregui I., Oliver R., Ballester J. L., Andries J., Goossens M., 2008a, ApJ, 679, 1611
Terradas J., Andries J., Goossens M., Arregui I., Oliver R., Ballester J. L., 2008b, ApJ, 687, L115
Timmer J., Koenig M., 1995, A&A, 300, 707
Tirry W. J., Berghmans D., 1997, A&A, 325, 329
Tirry W. J., Berghmans D., Goossens M., 1997, A&A, 322, 329
Tomczyk S., McIntosh S. W., Keil S. L., Judge P. G., Schad T., Seeley D. H., Edmondson J., 2007, Science, 317, 1192
van Ballegooijen A. A., Asgari-Targhi M., 2016, ApJ, 821, 106
van Ballegooijen A. A., Asgari-Targhi M., Cranmer S. R., DeLuca E. E., 2011, ApJ, 736, 3
Van Doorsselaere T. et al., 2020, Space Sci. Rev., 216, 140
Yuan D., Pascoe D. J., Nakariakov V. M., Li B., Keppens R., 2015, ApJ, 799, 221

This paper has been typeset from a TEX/LATEX file prepared by the author.